Quantitative Modeling of DNA-Mediated Electron Transfer between Metallointercalators

Eric J. C. Olson, Dehong Hu, Aldo Hörmann, and Paul F. Barbara*

Department of Chemistry, University of Minnesota, Minneapolis, Minnesota 55455

Received: October 10, 1996; In Final Form: November 11, 1996[⊗]

The distance dependence of electron transfer (ET) rates between donors and acceptors in a DNA environment has been an area of intense research and heated discussion, especially with regard to the recent report of ultrafast ET over a separation of >40 Å. This paper is focused on quantitative modeling of the photodynamics and gel electrophoresis/photocleavage experiments of the untethered DNA/metallointercalator system. Simulations are compared to previously published experimental results in order to quantitatively examine the possible involvement of long-range ET and donor/acceptor clustering in the DNA-mediated ET between metallointercalators. Comparison of the simulation results with a broad range of experimental data strongly indicates that a fairly typical distance dependence for ET ($\beta \approx 1$ Å^{-1}) coupled to donor/acceptor clustering is able to account for all features in the data and for related photocleavage studies.

I. Introduction

Electron transfer (ET) rate constants have been observed and predicted for a variety of media ranging from organics to proteins. To a very good approximation, ET rates are found to vary exponentially on the distance, R, between the electron donor and acceptor as follows:[1−8]

$$k_{ET}(R) = k_0 \exp[-\beta(R - R_0)], \quad (1)$$

where k_0 is defined as the ET rate constant for a donor/acceptor pair in closest contact, R_0. Experiment and theory have shown that β typically falls in the range of 0.8−1.5 Å^{-1}.

The distance dependence of ET rates between donors and acceptors in a DNA environment has been an area of intense research and heated discussion.[9−14] In particular, much of the attention has been focused on the surprising report of ultrafast ET over a large separation (>40 Å) between covalently-tethered metallointercalators (Ru(II) donors and Rh(III) acceptors), implying an extraordinarily shallow distance dependence ($\beta <$ 0.2 Å^{-1}) for ET in DNA.[15] Other reports of DNA-mediated ET have not observed a similarly shallow distance dependence,[16] demonstrating that long-range ET in DNA is not a general phenomenon.

A clear advantage of the tethered Ru/DNA/Rh system is that both the donor and acceptor are covalently held in a well-defined distance range.[15] ET kinetic studies with fixed donor/acceptor distances have been critical in establishing β for organic and biological systems and are certainly an important approach for studies of ET in DNA environments. On the other hand, the report on the tethered Ru/DNA/Rh system was limited by the exclusive use of steady-state emission spectroscopy, as opposed to time-resolved experiments. In particular, in the report by Murphy et al., an ET rate was estimated by using the apparent quenching of the Ru(II) metal-to-ligand charge transfer (MLCT) emission by the presence of the tethered Rh(III) acceptor.

Time-resolved absorption and emission experiments have proved to be critical in elucidating the mechanism and in measuring the kinetics of a variety of ET systems. In 1993 our group, in collaboration with Barton and co-workers, began an ultrafast time-resolved spectroscopy investigation of the Ru/DNA/Rh system. Initial attempts to study tethered samples were unsuccessful due to the facile photolysis of the samples and the limited available quantities. Unfortunately we have been forced to focus on the untethered metallointercalators in DNA. Earlier experiments on the noncovalent Ru/DNA/Rh system revealed very efficient luminescence quenching without the time resolution to resolve a majority of the quenching kinetics.[17]

Untethered samples possess a complex distribution of donor/acceptor separations rendering the ET kinetics of this system less ideal for studying long-range ET than tethered samples with fixed and large donor/acceptor distances. Nevertheless, the results on untethered samples can be analyzed to characterize the excited-state quenching process (presumably ET) and its apparent donor/acceptor distance dependence. Our time-resolved experiments have focused on the donor Δ-Ru(phen)$_2$dppz, the acceptor Δ-Rh(phi)$_2$bpy, and calf thymus DNA, but various other donors, acceptors, and types of DNA have been investigated. Previous papers, especially Arkin et al.,[18] describe the main experimental observations on the excited-state electron transfer kinetics $k_{ESET}(R)$ (eq 2), which occurs from the lowest lying MLCT state of the donor, and the recombination electron transfer kinetics $k_{RECET}(R)$ (eq 3).

$$Ru^{II}(phen)_2dppz(MLCT) + Rh^{III}(phi)_2bpy \xrightarrow[k_{ESET}]{} Ru^{III}(phen)_2dppz + Rh^{II}(phi)_2bpy \quad (2)$$

$$Ru^{III}(phen)_2dppz + Rh^{II}(phi)_2bpy \xrightarrow[k_{RECET}]{} Ru^{II}(phen)_2dppz + Rh^{III}(phi)_2bpy \quad (3)$$

The observed photodynamics were highly consistent with complete intercalation of the donor and acceptor in DNA. Efficient and rapid electron transfer was observed for photoexcited donors in the presence of acceptors, even at surprisingly low acceptor loading on the DNA duplex. The kinetics of the recombination reaction shows analogous trends. Both reactions exhibit a broad distribution of rates including a single fast (first-order) exponential component of ET and a distribution of substantially slower kinetic components. On a purely qualitative basis the photodynamics of the untethered Ru/DNA/Rh system can be alternatively interpreted as being evidence for rapid long-range ET with a shallow distance dependence or ET with an ordinary distance dependence combined with donor/acceptor clustering along the DNA strand (allowing for appreciable fast

* To whom correspondence should be addressed.

[⊗] Abstract published in *Advance ACS Abstracts,* January 1, 1997.

S1089-5647(96)03109-4 CCC: $14.00

ET even at low concentration).[18−20] However, it was argued that donor/acceptor clustering on the DNA is unlikely and inconsistent with electrophoresis measurements on the photocleavage of DNA by Rh(III) complexes investigated in both the absence and presence of Ru(II).[18]

This paper is focused on quantitative modeling of the previously reported experiments on the photodynamics of the Ru/DNA/Rh system and the gel electrophoresis/photocleavage experiments on this system.[18] No new experimental results are presented. A quantitative modeling scheme for electron transfer between intercalated donors and acceptors is described in detail for the first time. Preliminary reports of this model were made in 1994.[19] The simulation method involves two stages. First, an equilibrium distribution of donor and acceptor positions in the DNA is simulated from a rudimentary one-dimensional lattice model which includes a parameterized donor/acceptor interaction potential. The interaction potential allows for donor/acceptor clustering. Second, the simulated distribution of donor and acceptor positions is used as input for a calculation of the photodynamics invoking a phenomenological kinetic scheme and an assumed exponential distance dependence of the excited-state ET rate and the recombination ET rate. The simulations are compared to previously published experimental results in order to quantitatively examine the possible involvement of long-range ET and donor/acceptor clustering in the DNA-mediated ET reactions between metallointercalators.

II. Simulation Procedure

Intercalation of the donor and acceptor molecules in the DNA was simulated by Monte Carlo methods using a highly simplified effective potential and a one-dimensional lattice to represent DNA intercalation sites. The intercalation potential includes several independent terms. As indicated by experiment,[21] all simulations reported here assume intercalators are completely bound to the duplex and excluded from occupying nearest neighbor sites. Next-nearest neighbor sites could be assumed to have preferential stability so as to represent a clustering of donors and acceptors. This energetic stabilization is quantified by the parameter, P, which denotes preference for clustering. A value of unity indicates no preference. No intrinsic selectivity for intercalation at a particular site on the DNA is assumed in the majority of the simulations. However, some simulations were made with sequence selectivity and are described in a later section.

The Monte Carlo simulations were made with multiple strands (typically 32) and a sufficient number of Monte Carlo steps ($>10^4$) to ensure convergence on the equilibrium distribution. The strands were assumed to have identical length which was chosen to correspond to the average reported DNA length of the experimental samples. The Monte Carlo results were analyzed to give donor/acceptor nearest neighbor distributions, $\rho(R)$, for the discrete values of R that correspond to base-pair spacing, i.e. 3.4 Å/base-pair step.

Time-resolved emission kinetics, time-resolved absorption kinetics, and steady-state emission yields were calculated for specific $\rho(R)$ by assuming that each excited-state donor molecule exhibits independent photophysical behavior determined by its intrinsic radiative and nonradiative processes combined with the predicted ET kinetics (eq 1). Modeling the intrinsic radiative and nonradiative properties of the donor is complicated by the fact that even in the absence of quencher the excited-state decay of Δ-Ru(phen)$_2$dppz intercalated in DNA obeys biexponential kinetics dependent on the DNA loading. In the simulation, intrinsic decay rate constants were $k_i' = 1.16 \times 10^6\ s^{-1}$ and $k_i'' = 6.80 \times 10^6\ s^{-1}$ as determined by nanosecond-time-resolved-luminescence measurements.[22] The biexponential decays have been assigned to two distinct modes of intercalation of the Ru donor,[23] but this interpretation has been subject to serious doubt.[21] In the simulations here it was assumed that the quenching rate is independent of the intercalative binding mode. The excited-state population S at a certain time t was calculated employing the equation

$$S(t) = \sum_r \rho(R)(A'\, e^{-(k_i'+k_{ET}(R))t} + A''\, e^{-(k_i''+k_{ET}(R))t}) \quad (4)$$

where A' and A'' ($A' = 0.21$, $A'' = 0.79$ in all simulations) are the fractional populations of the two intrinsic decay rate constants and k_{ET} is the ET rate constant as defined by eq 1. For a specific set of DNA loadings, the only parameters required for a simulation of the emission data include the clustering preference P, β, and k_0.

The transient-absorption results are more complicated to simulate since multiple species may be absorbing at the probe wavelength. As previously described,[18] we will assume that the transient-absorption data roughly reflect the transient concentration of Δ-Ru(II) and thus reflect the recombination ET kinetics. The simulation of these data utilize identical P and β values as the emission simulation but introduce an independent k_0 representing the rate constant of recombination for donor/acceptor pairs in closest contact.

Simulation of the photocleavage results requires accounting for site-specific intercalator/DNA interactions and is described in a later section.

TABLE 1: Electron-Transfer Kinetic Models

model[a]	symbol	β (Å^{-1})	P	k_0(ESET) (ps^{-1})	k_0(RECET) (ps^{-1})
long-range ET	●	0.16[c]	1.0[b]	0.3[f]	0.3[g]
short-range ET	▼	1.0	1.0	0.3	0.01
clustering	♦	0.8[d]	13[e]	0.3	0.01

[a] Three kinetic limits are presented in order to simplify the comparison with experimental data. β and k_0 are defined by eq 1. [b] Preference for clustering, P, is defined in the Monte Carlo simulation by giving a randomly selected intercalation site a certain chance that it would be rejected (and a new site selected). Physically, the preference term relates the binding constant of a donor in the nearest available intercalation site adjacent to an intercalated acceptor to the binding constant of a donor in any other allowed intercalation site (e.g., non-nearest neighbor). [c] Given the lower limit of $k_0 \geq 3 \times 10^{10}\ s^{-1}$ for the rate of excited-state electron transfer established by TCSPC measurement,[18] $\beta \leq 0.16$ Å^{-1} must be assumed to account for the remarkable luminescence quenching reported for the tethered Ru/DNA/Rh sample[15] where donor/acceptor separation was fixed at ≈44 Å. [d] β values ranging from 0.6 to 1.4 Å^{-1} were investigated. β values less than 0.7 introduce dynamics in the predicted subnanosecond emission decays and transient-absorption recoveries not observed experimentally. β values greater than 1.0 predict insignificant nanosecond quenching components and cannot account for the overall emission quenching observed by steady-state luminescence spectroscopy. [e] P equal to 13 corresponds to a 13-fold increase in the probability of finding donors as near to acceptors as possible over finding them at any other position. The magnitude of P in our simulations translates into a free energy change ≈−1.5 kcal·mol^{-1} for transferring a donor from any non-nearest site to a nearest possible site adjacent to an acceptor. [f] Simulated quenching kinetics convolved with the TCSPC instrument-response function[18] indicate k_{ESET} must be $\geq 3 \times 10^{11}\ s^{-1}$ to account for the absence of decay dynamics in the TCSPC measurements. For the simulations, $(R - R_0)$ was assumed equal to $(n - 2) \times 3.4$ Å, where n corresponds to the number of intervening base steps. A molecular treatment would be necessary to more realistically calculate the edge-to-edge separations between donor and acceptor species. [g] k_{RECET} was selected to fit the observed fraction of subnanosecond MLCT bleach recovery at the lowest metallointercalator concentration.

III. Kinetic Simulations and Comparison to Experiment

We now consider the predicted experimental manifestations of the distance dependence of electron transfer and donor/

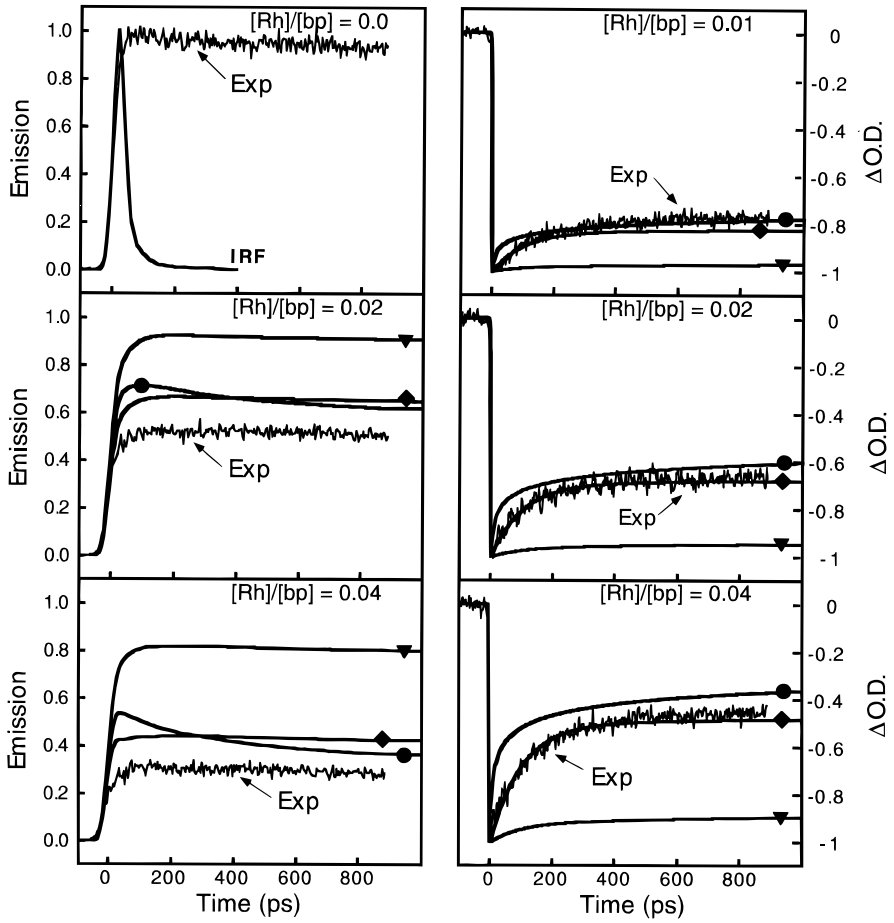

Figure 1. Picosecond experiment[18] and simulation on photoexcited Δ-Ru(phen)$_2$dppz bound to calf thymus DNA in the presence of various concentrations of Δ-Rh(phi)$_2$bpy. Simulation parameters are collected in Table 1. The solid triangle denotes the short-range ET, random-binding model. The solid circle denotes the long-range ET, random-binding model, and the solid diamond denotes the short-range ET, clustering model. The left-hand column represents the picosecond emission measurement and simulation obtained at 10 μM Ru, 500 μM bp calf thymus DNA. The upper panel displays the instrument-response function (IRF) and Ru/DNA emission data in the absence of Rh. The middle panel shows emission data and simulation for Ru/DNA in the presence of 10 μM Rh and the lower panel for 20 μM Rh. The right-hand column contains transient-absorption experiment and simulation obtained for 20 μM Ru, 1000 μM bp calf thymus DNA. The three concentrations of Rh shown are 10, 20, and 40 μM.

acceptor clustering according to the model introduced in the previous section. For comparison, the simulated results are presented with the previously published[18] experimental results. Three kinetic limits will be considered in order to simplify the comparison (see Table 1). The first model corresponds to long-range electron transfer. Simulation results from this model are represented by circles in Figures 1−3. The second electron transfer model possesses a typical distance dependence and is denoted in the figures with a triangle. The third model introduces donor/acceptor clustering, and simulated results are denoted with diamonds. For the first two models, β was fixed and k_0 values for the excited-state ET and recombination ET reactions were adjusted to give the best agreement with experiment. For the clustering model, agreement with experiment was generally very good and it was possible to refine the adjustable parameters β, P, and k_0 to fit the complete set of experimental data. The simulation parameters used to generate Figures 1−3 are summarized in Table 1.

The picosecond, nanosecond, and steady-state simulation results are compared to experiment in Figures 1−3. The long-range electron transfer model poorly agrees with each of the types of data. On the picosecond time scale it predicts resolvable emission decay not observed in experiment (Figure 1). Additionally, β values < 0.7 Å^{-1} predict multiple lifetimes in transient absorption in the $<$1000 ps time range, which is inconsistent with experiment (Figure 1). As a result, the overall quenching at times earlier than 10 ns is significantly overestimated by the long-range ET model, as shown in Figure 2. Finally, too much steady-state luminescence quenching is predicted by this model (Figure 3).

The set of simulations with $\beta = 1.0$ Å^{-1} and no preference for clustering of metallointercalators is also in poor agreement with experiment. Far too little excited-state ET (quenching) is predicted on the picosecond (Figure 1) and nanosecond (Figure 2) time scales. The predicted percent quenching for both the early-time emission and steady-state emission is far less than that observed over the entire range of acceptor concentrations (Figure 3). This behavior is a consequence of the small number of short-range donor/acceptor separations. Given the typical exponential decay of the ET rate with distance, only donor/acceptor pairs in close proximity can react sufficiently rapidly to contribute to the early-time dynamics. Nonpreferential binding of metallointercalators combined with a typical decay of the ET rate with distance cannot accurately predict experimental results.

In contrast, the electron-transfer model with a typical ET distance dependence coupled to donor/acceptor clustering predicts results that are in good agreement with the short and long time scale emission decay dynamics. Interestingly, the early-time emission quenching arises exclusively from donor/acceptor pairs bound to DNA with the shortest allowed separation. Donor/acceptor pairs separated by $> R_0$, the nearest allowed separation, are predicted to make only a minor contribution to the observed emission decays. Very recently, Nordén

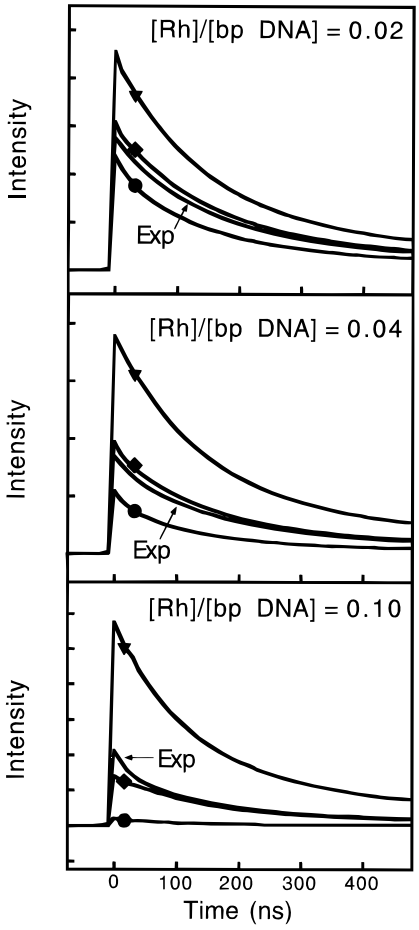

Figure 2. Nanosecond emission experiment[22] and simulation on photoexcited Δ-Ru(phen)$_2$dppz bound to calf thymus DNA in the presence of various concentrations of Δ-Rh(phi)$_2$bpy. Simulation parameters are collected in Table 1. The solid triangle denotes the short-range ET, random binding model. The solid circle denotes the long-range ET, random binding model, and the solid diamond denotes the short-range ET, clustering model. Emission quenching data on 10 μM Ru, 500 μM bp calf thymus DNA in the presence of 10 μM (top), 20 μM (middle), and 50 μM (bottom) Rh.

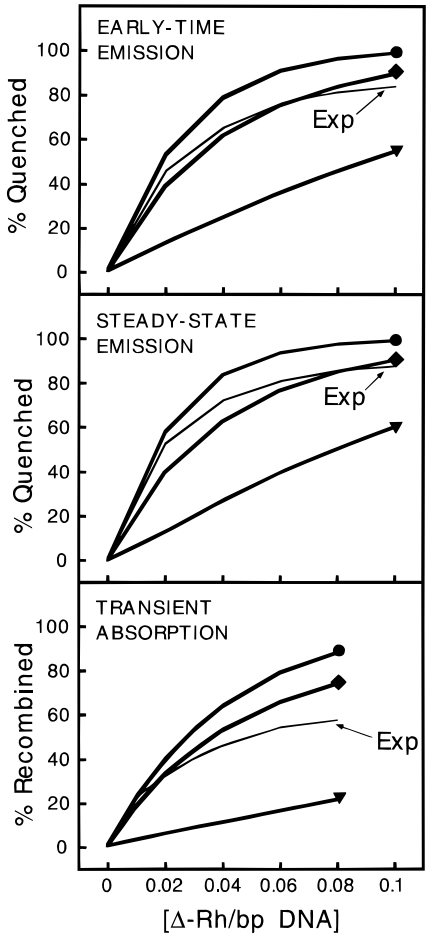

Figure 3. Fractional quenching and recombination experiment[22] and simulation on photoexcited Δ-Ru(phen)$_2$dppz bound to calf thymus DNA in the presence of various concentrations of Δ-Rh(phi)$_2$bpy. Simulation parameters are collected in Table 1. The solid triangle denotes the short-range ET, random binding model. The solid circle denotes the long-range ET, random binding model, and the solid diamond denotes the short-range ET, clustering model. The top panel displays early-time emission quenching (<10 ns), and the middle panel displays the total integrated emission intensity on 10 μM Ru, 500 μM bp calf thymus DNA in the presence of various concentrations of Rh. The lower panel displays the fraction of photoinduced Ru(II)-MLCT bleach recovery within 1 ns.

and co-workers have arrived at a similar (clustering) model for the ET quenching of Ru(phen)$_2$dppz emission by Rh(phi)$_2$bpy on DNA.[24]

The failure of the long-distance electron transfer model and the typical distance dependence model with no clustering preference is even more apparent when one considers the ps transient-absorption data which monitors the recombination ET (Figure 1). The model with preferential clustering is in excellent agreement with experiment. Both the fraction of fast recombination and the shape of the recombination kinetics are predicted within experimental uncertainty. The other two models fail dramatically.

IV. Photocleavage Studies and Sequence-Specific Intercalation

Barton and co-workers have made extensive investigations of the sequence selectivity of Rh(III) intercalated in DNA by a photocleavage assay method.[18,25,26] For example, gel electrophoresis measurements of DNA photocleaved by Δ-Rh(phi)$_2$bpy are shown in Figure 4 in the absence and presence of Δ-Ru(phen)$_2$dppz. These results are reproduced from Arkin et al. and correspond to phosphorimager scans of a 180-bp [3′-^{32}P]-end-labeled DNA restriction fragment.[18] The intensity in Figure 4 has been assumed to roughly correlate with preference for binding at a specific site on the DNA fragment, convoluted with the site selectivity of the photocleavage and other aspects of the photochemistry. Arkin et al. have argued that the absence of a significant change in the photocleavage pattern in the presence of Ru(phen)$_2$dppz is qualitative evidence that the donor/acceptor species do not possess a preference for clustering on DNA. In particular, they argue that the cleavage by Rh(phi)$_2$bpy in its preferred sites would become even more intense in the presence of Ru(phen)$_2$dppz.

In an attempt to determine the actual sensitivity of the photocleavage studies to nearest neighbor clustering, we have added DNA sequence preference to our Monte Carlo procedure and used this method to simulate intercalator/DNA interactions, in addition to donor/acceptor interactions, and predict the photocleavage experiments. It was assumed that the experimental intensity in the photocleavage data was an approximate measure of the site occupancy of Δ-Rh(phi)$_2$bpy. Our sequence-specific intercalator/DNA interaction potential was taken directly from the published gel electrophoresis data.[18] Monte Carlo simulations including this sequence-specific potential were used to determine a distribution of Δ-Rh(phi)$_2$bpy site occupancies and these occupancies, were assumed to simply reflect the probability of cleaving at a particular site.

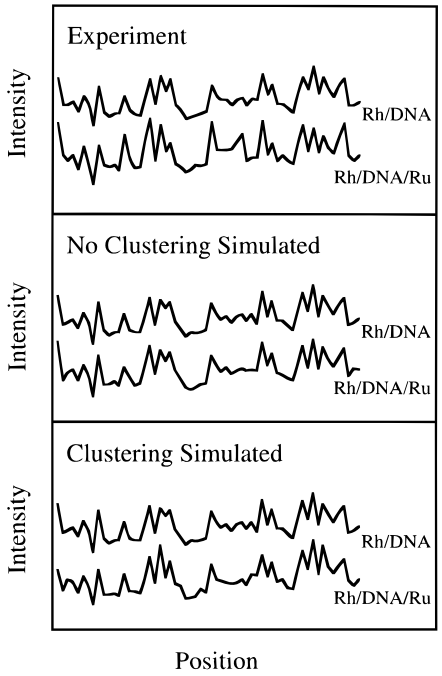

Figure 4. Gel electrophoresis experiments and simulations on DNA photocleavage by Δ-Rh(phi)$_2$bpy. Shown are a portion of phosphorimager scans on a DNA restriction fragment. The upper panel contains experimental results[18] on photocleavage of 500 μM bp DNA with 10 μM Δ-Rh(phi)$_2$bpy in the presence (bottom) and absence (top) of 10 μM Δ-Ru(phen)$_2$dppz. Monte Carlo simulation results at equivalent concentrations with no preferential intercalator/intercalator interactions are displayed in the middle panel. The lower panel displays Monte Carlo simulation results with clustering ($P = 13$), at identical metallointercalator concentrations.

Simulations of the photocleavage of DNA by Δ-Rh(phi)$_2$bpy in the absence and presence of Δ-Ru(phen)$_2$dppz shows that at sufficiently low loading of intercalators (the conditions under which the photocleavage experiments were performed), the site occupancy simply reflects the sequence-specific potential and no intercalator/intercalator interactions.

In order to investigate the consequence of preferential clustering on the phosphorimager scan, a simulation was made with the nearest neighbor preference derived above. The predicted phosphorimager scans, both in the absence and presence of clustering, are very similar to experiment and nearly indistinguishable from each other (Figure 4). Consequently, these simulations strongly suggest that the photocleavage assay is not a sensitive measure for donor/acceptor clustering.

We have also explored the consequence of sequence specificity of the intercalation on the electron transfer kinetics. Using the site-specific probability distributions in Figure 4, for both donor and acceptors, simulations of the type shown in Figures 1−3 were made. The results are nearly identical to the simulations described above which assumed that there was not a significant sequence selectivity. Therefore, the basic conclusions of the previous section of this paper are not altered by sequence-specific binding.

V. Conclusions and Summary

A quantitative analysis of the previously reported experiments on the photodynamics of the Δ-Ru/DNA/Δ-Rh system and the gel electrophoresis/photocleavage experiments has been made using a simulation procedure for electron transfer between intercalated donors and acceptors. An equilibrium distribution of donor and acceptor positions in the DNA was simulated from a rudimentary one-dimensional lattice model for intercalation which allows for variable donor/acceptor clustering and sequence selectivity. The simulated distribution of donor and acceptor positions was used as input for a calculation of the photodynamics invoking a phenomenological kinetic scheme and an assumed exponential distance dependence of the excited-state ET rate and the recombination ET rate. Comparison of the simulation results with a broad range of experimental data strongly indicate that a fairly typical distance dependence for ET ($\beta \approx 1$ Å^{-1}) coupled to donor/acceptor clustering is able to account for all features in the data and for related photocleavage studies. In contrast, simulation with $\beta < 0.7$ Å^{-1}, corresponding to long-range ET, is not able to account for the data. These simulations emphasize the importance of well-defined donor/acceptor separations in studies of electron transfer, particularly in the absence of independent information about specific donor/acceptor interactions.

Note Added in Proof. After this paper was accepted, we received a preprint (Lincoln, P.; Tuite, E.; Nordén, B. *J. Am. Chem. Soc.*, in press) that presents conclusions similar to ours.

Acknowledgment. This work was supported by the Department of Energy, Office of Basic Energy Science, Division of Chemical Science, and the National Science Foundation. E.J.C.O. is supported by a NIH training grant, and A.H. thanks the Swiss National Science Foundation for a postdoctoral grant.

References and Notes

(1) Ratner, M. A. *J. Phys. Chem.* **1990**, *94*, 4877.
(2) McLendon, G. *Acc. Chem. Res.* **1988**, *21*, 160.
(3) Beratan, D. N.; Betts, J. N.; Onuchic, J. N. *Science* **1991**, *252*, 1285.
(4) Wasielewski, M. R. *Chem. Rev.* **1992**, *92*, 435.
(5) Wuttke, D. S.; Bjerrum, M. J.; Chang, I.-J.; Winkler, J. R.; Gray, H. B. *Biochim. Biophys. Acta* **1992**, *1101*, 168.
(6) Turro, N. J.; Barton, J. K.; Tomalia, D. A. *Acc. Chem. Res.* **1991**, *24*, 332.
(7) Barbara, P. F.; Meyer, T. J.; Ratner, M. A. *J. Phys. Chem.* **1996**, *100*, 13148.
(8) Newton, M. D. *Chem. Rev.* **1991**, *91*, 767.
(9) Meade, T. J.; Kayyem, J. F. *Angew. Chem., Int. Ed. Engl.* **1995**, *34*, 352.
(10) Meade, T. J. In *Metal Ions in Biological Systems*; Sigel, H., Sigel, A., Eds.; Marcel Deckker, Inc.: New York, 1995; Vol. 33, Chapter 13.
(11) Stemp, E. D. A.; Barton, J. K. In *Metal Ions in Biological Systems*; Sigel, H., Sigel, A., Eds.; Marcel Deckker, Inc.: New York, 1995; Vol. 33, Chapter 11.
(12) Felts, A. K.; Pollard, W. T.; Friesner, R. A. *J. Phys. Chem.* **1995**, *99*, 2929.
(13) Priyadarshy, S.; Risser, S. M.; Beratan, D. N. *J. Phys. Chem.* **1996**, *100*, 17678.
(14) Risser, S. M.; Beratan, D. N.; Meade, T. J. *J. Am. Chem. Soc.* **1993**, *115*, 2508.
(15) Murphy, C. J.; Arkin, M. R.; Jenkins, Y.; Ghatlia, N. D.; Bossmann, S.; Turro, N. J.; Barton, J. K. *Science* **1993**, *262*, 1025.
(16) Brun, A. M.; Harriman, A. *J. Am. Chem. Soc.* **1992**, *114*, 3656.
(17) Murphy, C. J.; Arkin, M. R.; Ghatlia, N. D.; Bossmann, S.; Turro, N. J.; Barton, J. K. *Proc. Natl. Acad. Sci. U.S.A.* **1994**, *91*, 5315.
(18) Arkin, M. R.; Stemp, E. D. A.; Holmlin, R. E.; Barton, J. K.; Hörmann, A.; Olson, E. J. C.; Barbara, P. F. *Science* **1996**, *273*, 475.
(19) Hörmann, A.; Olson, E. J. C.; Barbara, P. F.; Stemp, E. D. A.; Arkin, M. R.; Barton, J. K. *Abstr. Pap. -Am. Chem. Soc.* **1994**, *208*, 385-PHYS.
(20) Olson, E. J. C.; Hörmann, A.; Barbara, P. F.; Stemp, E. D. A.; Arkin, M. R.; Barton, J. K. *Abstr. Pap. -Am. Chem. Soc.* **1995**, *210*, 344-PHYS.
(21) Hiort, C.; Lincoln, P.; Nordén, B. *J. Am. Chem. Soc.* **1993**, *115*, 3448.
(22) Arkin, M. R.; Stemp, E. D. A.; Turro, C.; Turro, N. J.; Barton, J. K. *J. Am. Chem. Soc.* **1996**, *118*, 2267.
(23) Jenkins, Y.; Friedman, A. E.; Turro, N. J.; Barton, J. K. *Biochemistry* **1992**, *31*, 10809.
(24) Tuite, E. Personal communication, 1996.
(25) Chow, C. S.; Barton, J. K. In *DNA Structures Part B: Chemical and Electrophoretic Analysis of DNA*; Lilley, D. M. J., Dahlberg, J. E., Eds.; Academic Press, Inc.: San Diego, CA, 1992; *Vol. 212*, p 219.
(26) Sitlani, A.; Barton, J. K. *Biochemistry* **1994**, *33*, 12100.